



HAL
open science

Neurog2 Deficiency Uncovers a Critical Period of Cell Fate Plasticity and Vulnerability among Neural-Crest-Derived Somatosensory Progenitors

Stéphanie Ventéo, Simon Desiderio, Pauline Cabochette, Alexandre Deslys, Patrick Carroll, Alexandre Pattyn

► **To cite this version:**

Stéphanie Ventéo, Simon Desiderio, Pauline Cabochette, Alexandre Deslys, Patrick Carroll, et al.. Neurog2 Deficiency Uncovers a Critical Period of Cell Fate Plasticity and Vulnerability among Neural-Crest-Derived Somatosensory Progenitors. Cell Reports, 2019, 29 (10), pp.2953-2960.e2. 10.1016/j.celrep.2019.11.002 . hal-03063996

HAL Id: hal-03063996

<https://hal.science/hal-03063996>

Submitted on 31 May 2021

HAL is a multi-disciplinary open access archive for the deposit and dissemination of scientific research documents, whether they are published or not. The documents may come from teaching and research institutions in France or abroad, or from public or private research centers.

L'archive ouverte pluridisciplinaire **HAL**, est destinée au dépôt et à la diffusion de documents scientifiques de niveau recherche, publiés ou non, émanant des établissements d'enseignement et de recherche français ou étrangers, des laboratoires publics ou privés.

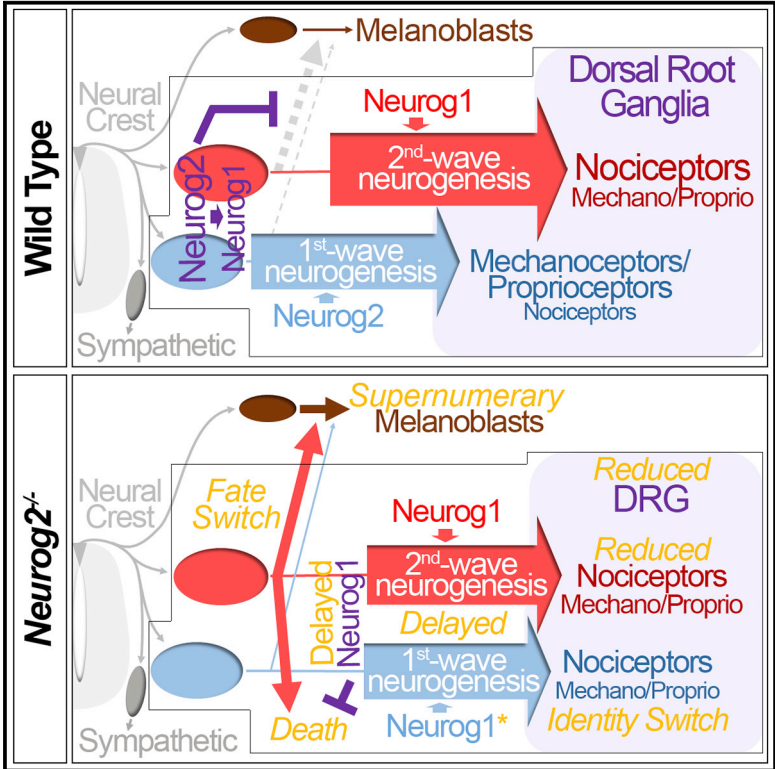


Distributed under a Creative Commons Attribution - NonCommercial - NoDerivatives 4.0 International License

Cell Reports

Neurog2 Deficiency Uncovers a Critical Period of Cell Fate Plasticity and Vulnerability among Neural-Crest-Derived Somatosensory Progenitors

Graphical Abstract



Authors

Stéphanie Ventéo, Simon Desiderio, Pauline Cabochette, Alexandre Deslys, Patrick Carroll, Alexandre Pattyn

Correspondence

alexandre.pattyn@inserm.fr

In Brief

Ventéo et al. report that in contrast to cervical levels, trunk dorsal root ganglia of *Neurog2*^{-/-} mutants contain reduced numbers of all somatosensory neuron subtypes due to multiple defects in neural-crest-derived progenitors—including sensory-to-melanocyte fate switch, apoptosis, and delayed differentiation—that affect the accuracy of the successive waves of neurogenesis.

Highlights

- *Neurog2*^{-/-} mutant trunk DRGs contain reduced numbers of all sensory neuron subtypes
- *Neurog2* influences the onset and accuracy of the successive sensory neurogenic waves
- Pools of *Neurog2*-deficient sensory progenitors either die or become melanoblasts
- *Neurog2* deficiency illustrates cell fate plasticity and vulnerability among NCCs



Neurog2 Deficiency Uncovers a Critical Period of Cell Fate Plasticity and Vulnerability among Neural-Crest-Derived Somatosensory Progenitors

Stéphanie Ventéo,¹ Simon Desiderio,^{1,2} Pauline Cabochette,^{1,2} Alexandre Deslys,¹ Patrick Carroll,¹ and Alexandre Pattyn^{1,3,*}

¹Institute for Neurosciences of Montpellier, University of Montpellier, INSERM U1051, 80 rue Augustin Fliche, 34091 Montpellier, France

²These authors contributed equally

³Lead Contact

*Correspondence: alexandre.pattyn@inserm.fr
<https://doi.org/10.1016/j.celrep.2019.11.002>

SUMMARY

Functionally distinct classes of dorsal root ganglia (DRG) somatosensory neurons arise from neural crest cells (NCCs) in two successive phases of differentiation assumed to be respectively and independently controlled by the proneural genes *Neurog2* and *Neurog1*. However, the precise role of *Neurog2* during this process remains unclear, notably because no neuronal loss has been reported hitherto in *Neurog2*^{-/-} mutants. Here, we show that at trunk levels, *Neurog2* deficiency impairs the production of subsets of all DRG neuron subtypes. We establish that this phenotype is highly dynamic and reflects multiple defects in NCC-derived progenitors, including somatosensory-to-melanocyte fate switch, apoptosis, and delayed differentiation which alters neuronal identity, all occurring during a narrow time window when *Neurog2* temporarily controls onset of *Neurog1* expression and neurogenesis. Collectively, these findings uncover a critical period of cell fate plasticity and vulnerability among somatosensory progenitors and establish that *Neurog2* function in the developing DRG is broader than initially envisaged.

INTRODUCTION

Our ability to detect and process mechanical, proprioceptive, thermal, or noxious information relies on the somatosensory nervous system. At trunk levels, the primary receptors of this system, located in the dorsal root ganglia (DRG), form a heterogeneous population of functionally specialized neurons whose diversity is largely established early during embryogenesis (Lallemend and Ernfors, 2012). DRG neurons arise from neural crest cells (NCCs) that also contribute at this axial level to sympathetic neurons, glial cells, smooth muscles, or melanocytes. Lineage segregation among NCCs involves time- and environment-dependent changes in their developmental competence, notably through the induction of specific transcriptional regulators

(Pavan and Raible, 2012; Dupin and Sommer, 2012; Bhatt et al., 2013). The bHLH transcription factors *Neurog2* and *Neurog1* are early markers of the somatosensory lineage (Sommer et al., 1996) in which they orchestrate neuronal differentiation presumably by respectively and independently controlling two successive waves of neurogenesis. It is indeed assumed that a first group of progenitors differentiates between embryonic day 9.5 (E9.5) and E11.5 under the control of *Neurog2* to generate mechano/proprioceptors as well as few large-diameter nociceptors, whereas a second group arising slightly later from NCCs, either directly or indirectly by the boundary cap cells, differentiates between E10.5 and E13.5 under the control of *Neurog1* to mainly produce small-diameter nociceptors (Figure S1A; Lawson and Biscoe, 1979; Frank and Sanes, 1991; Ma et al., 1999; Maro et al., 2004; George et al., 2010; Bachy et al., 2011; Ohayon et al., 2015). This model is supported by the phenotypes of *Neurog1*^{-/-};*Neurog2*^{-/-} double knockouts (dKOs) in which no DRG neuron is ever produced and of *Neurog1*^{-/-} mutants in which late-born small nociceptors are specifically absent. In contrast, direct evidence for a specific role of *Neurog2* during the first neurogenic wave remains elusive, notably because no neuronal loss has been reported in *Neurog2*^{-/-} mutants at cervical levels (Ma et al., 1999). Here, we show that at trunk levels, *Neurog2* deficiency affects the genesis of subsets of all DRG neuron subtypes as the result of multiple defects in pools of first- and second-wave somatosensory progenitors.

RESULTS AND DISCUSSION

First-Wave Somatosensory Progenitors Mainly Form Nociceptors in the Absence of *Neurog2* Function

We previously characterized *DBZEB;Wnt1Cre;Egr2*^{DT/+} (*DWE*) transgenic mice in which concomitant overexpression of a dominant-negative form of ZEB1/2 proteins in NCCs and genetic ablation of boundary cap cells triggered the early complete elimination of second-wave somatosensory progenitors at thoracic levels, while largely sparing those of the first wave (Figures S1A and S1B; Ohayon et al., 2015). In these animals, DRG neurogenesis, assessed by transient *NeuroD* expression, started on time but prematurely ended at E11.5 (Figures 1A, 1B, and 1D), consistent with the entire depletion of *Neurog1*-positive (+) second-wave progenitors from this stage (Figures 1A, 1B, and 1E). In



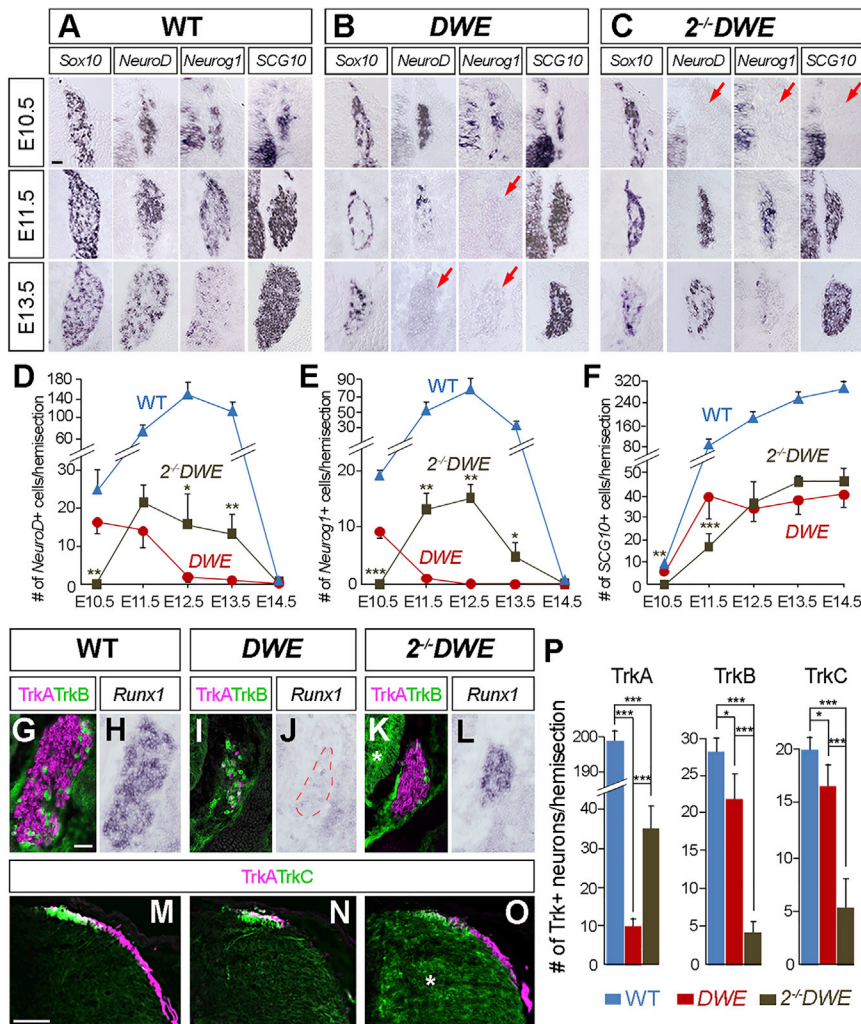


Figure 1. First-Wave Somatosensory Progenitors Mainly Form Nociceptors in the Absence of *Neurog2* Function

(A–C) Representative images of *in situ* hybridizations for *Sox10*, *NeuroD*, *Neurog1*, and *SCG10* on thoracic DRG transverse sections from WT (A), *DBZEB;Wnt1Cre;Egr2^{DT/+}* (DWE; B), and *Neurog2^{-/-};DBZEB;Wnt1Cre;Egr2^{DT/+}* (*2^{-/-}DWE*; C) embryos at E10.5, E11.5, and E13.5. In panels without staining, the position of the DRG is indicated by a red arrow. Scale bar, 50 μ m.

(D–F) Quantitative time-course analyses of *NeuroD*+ differentiating precursors (D), *Neurog1*+ sensory progenitors (E), and *SCG10*+ post-mitotic neurons (F) between E10.5 and E14.5 in WT (blue curve), DWE (red curve), and *2^{-/-}DWE* (brown curve) embryos. At least three animals for each genotype were analyzed, except at E14.5 where two DWE and two *2^{-/-}DWE* embryos were counted. Data are represented as means \pm SEM. Statistical differences between DWE and *2^{-/-}DWE* animals are indicated. **p* < 0.05; ****p* < 0.001.

(G–O) Representative images of double-immunofluorescence staining for TrkA and TrkB (G, I, and K) or for TrkA and TrkC (M–O) at E13.5 and of *in situ* hybridizations for *Runx1* at E12.5 (H, J, and L) on transverse sections of the thoracic DRG (G–L) or of the dorsal root entry zone (M–O) from WT (G, H, and M), DWE (I, J, and N), or *2^{-/-}DWE* (K, L, and O) mice. Asterisks in (K) and (O) point to GFP signal from the *Neurog2* locus. Scale bars, 50 μ m. (P) Quantitative analyses of TrkA+, TrkB+, or TrkC+ sensory neurons at E13.5 in WT (blue columns; *n* = 7), DWE (red columns; *n* = 9), and *2^{-/-}DWE* (brown columns; *n* = 5) embryos. Data are represented as means \pm SEM. **p* < 0.05; ****p* < 0.001. See also Figure S1.

turn, numbers of *SCG10*+ neurons reached a maximum as early as E11.5 and were reduced by 85% (\pm 1.3%) compared to wild type (WT) at E14.5 (Figures 1A, 1B, and 1F), reflecting agenesis of late-born TrkA+ small nociceptors (Figures 1G, 1I, and 1P; Figures S1A, S1B, S1D, and S1E). This model, thus, represented a good opportunity to assess the behavior of first-wave progenitors in the absence of *Neurog2* function by studying *Neurog2^{-/-};DBZEB;Wnt1Cre;Egr2^{DT/+}* (*2^{-/-}DWE*) compound mutants. In E10.5 *2^{-/-}DWE* embryos, despite the presence of many *Sox10*+ NCCs in the DRG primordia, expression of *Neurog1* and overt signs of neuronal differentiation were initially absent (Figures 1C–1F), supporting a key role for *Neurog2* in triggering *Neurog1* expression and neurogenesis in first-wave progenitors. Strikingly, however, between E10.5 and E11.5, neurogenesis eventually started in these animals and continued until E13.5, which correlated with a second, *Neurog2*-independent, phase of *Neurog1* expression (Figures 1C–1E). In turn, *SCG10*+ neurons appeared in a delayed manner from E11.5, and their numbers increased until E13.5 to reach a plateau comparable to DWE embryos, albeit shifted in time, representing 18.4%

(\pm 2.85%) of the normal DRG contingent at E14.5 (Figures 1C and 1F). Furthermore, an analysis of the neuronal subtypes generated in *2^{-/-}DWE* embryos revealed a striking increase of TrkA+ nociceptors and a concomitant decrease of TrkB+ and TrkC+ mechano/proprioceptors compared to DWE animals (Figures 1G, 1I, and 1K; Figures S1D–S1F). This was evocative of an identity switch also observable at the level of the dorsal root entry zone (Figures 1M–1O). In line with this, although expression of the late-born nociceptors determinant *Runx1* (Chen et al., 2006) was virtually absent in DWE embryos, it was recovered in *2^{-/-}DWE* animals (Figures 1H, 1J, and 1L). Therefore, without excluding that few first-wave progenitors might be depleted in the absence of *Neurog2* function (see Ma et al., 1999 and Figure 4L), these data show that a large proportion is temporarily maintained and subsequently differentiates in a delayed manner through the compensatory action of *Neurog1* to produce mainly nociceptors instead of mechano/proprioceptors (Figure S1C). This “intra-lineage” switch combined with the loss of small nociceptors in *Neurog1^{-/-}* mutants (Ma et al., 1999) suggests that beyond its proneural role, *Neurog1* might also participate in specifying the nociceptive identity. Alternatively, although not exclusively, this switch may be the consequence

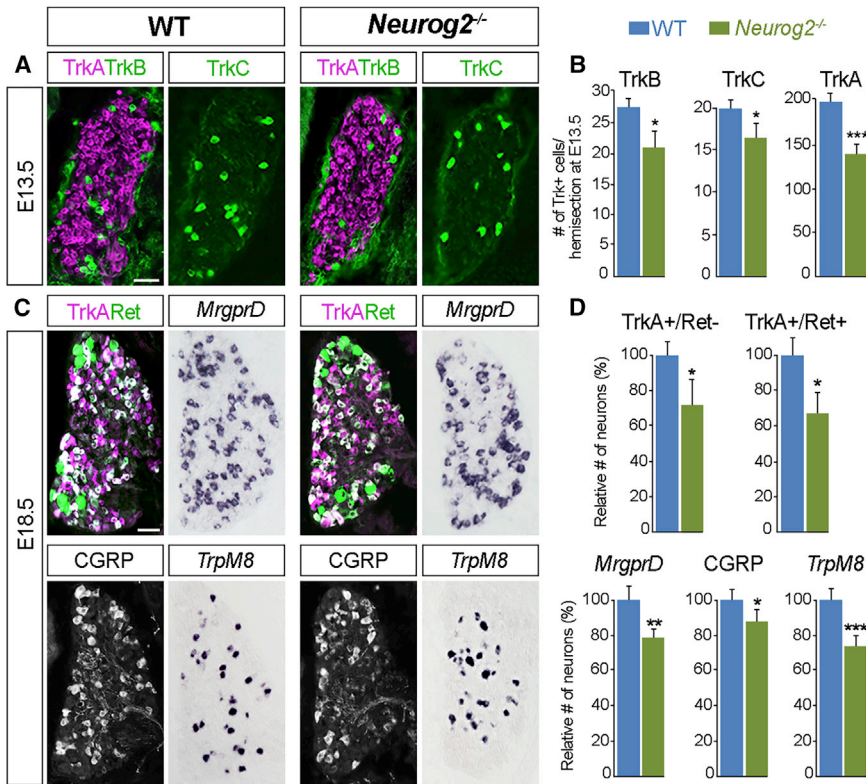


Figure 2. Thoracic DRG of *Neurog2*^{-/-} Mutants Contain Reduced Numbers of All Neuronal Subtypes

(A) Representative images of immunofluorescence staining for TrkA and TrkB or for TrkC at E13.5 on thoracic DRG transverse sections of WT and *Neurog2*^{-/-} mutants.

(B) Quantification of Trk⁺ neurons in WT (blue bars; n = 7) and *Neurog2*^{-/-} (green bars; n = 7) embryos at E13.5. Data are represented as means ± SEM. *p < 0.05; ***p < 0.001.

(C) Representative images of immunofluorescence staining for TrkA and Ret or for CGRP and of *in situ* hybridizations for *MrgprD* and *TrpM8* on thoracic DRG transverse sections of WT and *Neurog2*^{-/-} mutants at E18.5. Scale bar, 50 μm.

(D) Relative quantification of the peptidergic TrkA⁺/Ret⁻ and non-peptidergic TrkA⁺/Ret⁺ populations and of *MrgprD*⁺, CGRP⁺ and *TrpM8*⁺ nociceptor subtypes in WT (blue bars; n = 6) and *Neurog2*^{-/-} (green bars; n = 8) embryos at E18.5. Data are represented as means ± SEM. *p < 0.05; **p < 0.01; ***p < 0.001.

of differentiation delay and reflect that distinct environmental cues at different stages influence the formation of specific neuronal subtypes (Moqrich et al., 2004; Bhatt et al., 2013; Hadjab et al., 2013). In this case, *Neurog1/2* would ensure an accurate timing of differentiation but not necessarily an identity, implying that other determinants, such as *Prdm12* in the nociceptive lineage (Bartesaghi et al., 2019; Desiderio et al., 2019), control the latter aspect. Further studies are nonetheless needed to definitely solve this issue.

Thoracic DRG of *Neurog2*^{-/-} Mutants Contain Reduced Numbers of All Neuronal Subtypes

These observations raised the possibility that thoracic DRG of *Neurog2*^{-/-} mutants may contain fewer mechano/proprioceptors but supernumerary nociceptors. Analyses of *Neurog2*^{-/-} embryos at E13.5 revealed that numbers of TrkB⁺ and TrkC⁺ mechano/proprioceptors were indeed reduced by 25% (±9.3%) and 17% (±11.3%), respectively (Figures 2A and 2B). Unexpectedly however, we also found a drastic 29.6% (±3.8%) reduction of TrkA⁺ neurons (Figures 2A and 2B). This could not simply reflect a deficit of early-born large-diameter nociceptors, which represent only 10% of the entire TrkA⁺ population (Chen et al., 2006; Lallemand and Ernfors, 2012), suggesting that late-born small-diameter nociceptors were affected. Analyses at E18.5, when the latter population is being segregated into “peptidergic” and “non-peptidergic” classes, respectively TrkA⁺/Ret⁻ and TrkA⁺/Ret⁺ at this stage (Chen et al., 2006; Liu and Ma, 2011; Lallemand and Ernfors, 2012), showed that both classes were reduced by 29% (±15.3%)

and 32.5% (±13.3%), respectively, in the mutants (Figures 2C and 2D). In line with this, numbers of nociceptor subtypes expressing *MrgprD*, CGRP, or *Trpm8* (Liu and Ma, 2011) were all decreased by 26.4% (±5.6%; n = 8), 12% (±6.4%), and 26.8% (±6.4%), respectively (Figures 2C and 2D). These data, thus, show that at thoracic levels, *Neurog2* deficiency affects subsets of all somatosensory neuron subtypes, including populations of late-born nociceptors. It is of note that although similar results were found at abdominal levels (not shown), they contrast with previous data at cervical levels (Ma et al., 1999; see below).

Neurog2 Deficiency Generally Impairs Neurogenesis in Trunk DRG

Reduced numbers of mechano/proprioceptors in the trunk DRG of *Neurog2*^{-/-} mutants could logically be explained by the developmental switch undergone by first-wave progenitors. In contrast, deficiency of late-born nociceptors was *a priori* counterintuitive, except if the second neurogenic wave was also altered. To test this, we performed a time-course analysis of DRG neurons formation. At E10.5, when the first neurogenic wave is ongoing and the second has started (Lawson and Biscoe, 1979; Ma et al., 1999), *Neurog2*^{-/-} mutants could be considered as *Neurog1*^{-/-}; *Neurog2*^{-/-} dKOs because *Neurog1* expression was undetectable and neuronal differentiation was impaired, despite the presence of numerous *Sox10*⁺ NCCs in the coalescing DRG (Figures 3A–3D and 3F). This shows that *Neurog2* generally controls an initial phase of *Neurog1* expression and onset of neurogenesis also in second-wave progenitors. It also indicates that invasion of the DRG primordia by NCCs is largely *Neurog1/2* independent (see also Figure 4N). By E11.5, however, *Neurog1* was eventually induced in the mutants and neurogenesis was initiated and continued until E13.5, as in WT (Figures 3A–3E). Nevertheless, at

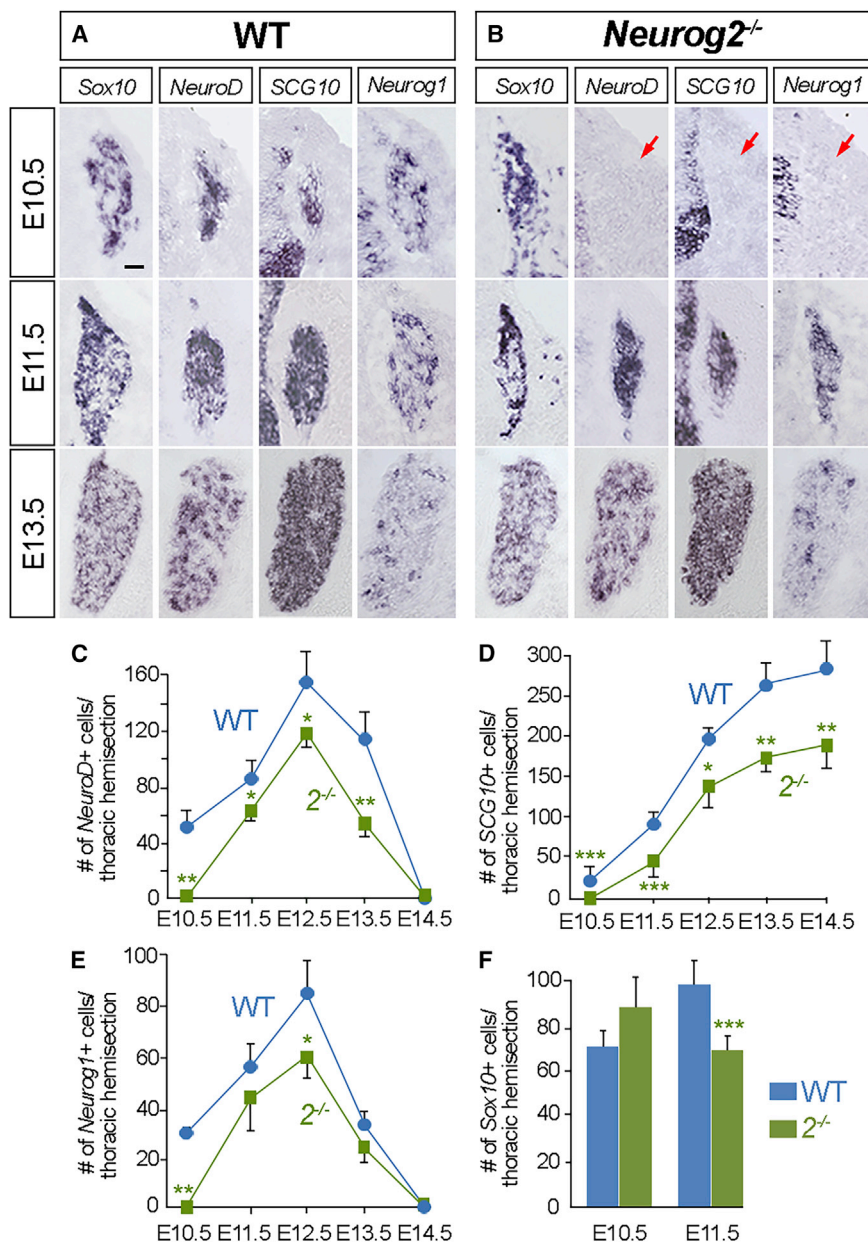


Figure 3. *Neurog2* Deficiency Generally Impairs Neurogenesis in Trunk DRG

(A and B) Representative images of *in situ* hybridizations for *Sox10*, *NeuroD*, *SCG10*, and *Neurog1* on thoracic DRG transverse sections from WT (A) and *Neurog2*^{-/-} embryos (B) at E10.5, E11.5, and E13.5. Arrows in (B) point to the position of the DRG primordia revealed by *Sox10* expression on adjacent sections. Scale bar, 50 μ m.

(C–E) Quantitative time-course analyses of *NeuroD*⁺ differentiating precursors (C), *SCG10*⁺ post-mitotic neurons (D), and *Neurog1*⁺ sensory progenitors (E) between E10.5 and E14.5 in WT (blue curve) and *Neurog2*^{-/-} embryos (2^{-/-}, green curve). For each genotype, at least 3 embryos were analyzed at all stages. Data are represented as means \pm SEM. **p* < 0.05; ***p* < 0.01; ****p* < 0.001.

(F) Quantification of *Sox10*⁺ cells at E10.5 and E11.5 in thoracic DRG of WT (blue columns; *n* = 4 at E10.5 and *n* = 8 at E11.5) and *Neurog2*^{-/-} embryos (2^{-/-}, green columns; *n* = 5 at E10.5 and *n* = 10 at E11.5). Data are represented as means \pm SEM. ****p* < 0.001.

See also Figures S2 and S4.

all stages, numbers of *NeuroD*⁺ precursors and of *SCG10*⁺ neurons were reduced compared to WT (Figures 3C and 3D), leading to a 34.48% (\pm 6.17%) decrease of the whole DRG contingent at E14.5 (Figure 3D). This was notably evident at E12.5 when the production of late-born nociceptors normally peaks (Figures 3C; Lawson and Biscoe, 1979; Ma et al., 1999). Therefore, and also taking into account that most mutant first-wave progenitors atypically differentiate concomitantly to second-wave progenitors (Figure 1), these data indicate that *Neurog2* deficiency perturbs the normal course of the second *Neurog1*-dependent neurogenic wave, an issue further supported by extrapolated dissociation of the two neurogenic waves in WT versus *Neurog2*^{-/-} embryos (Figures S2A and S2B).

mainly concerned second-wave progenitors (Figure S2D). Altogether, these data show that *Neurog2* deficiency generally impairs DRG neurogenesis, not only from the first wave whose timing and accuracy are altered but also from the second wave which is affected in two ways: (1) its onset is also delayed due to postponed induction of *Neurog1*, and (2) it is eventually initiated from a smaller progenitor reservoir that appears specifically depleted between E10.5 and E11.5.

In parallel, lineage analyses based on the great stability of the GFP protein expressed from the *Neurog2* locus (Figure S2E; Andersson et al., 2006) supported that *Neurog2* was not only expressed in first-wave progenitors but also transiently in a significant proportion of second-wave progenitors (Figure S2F),

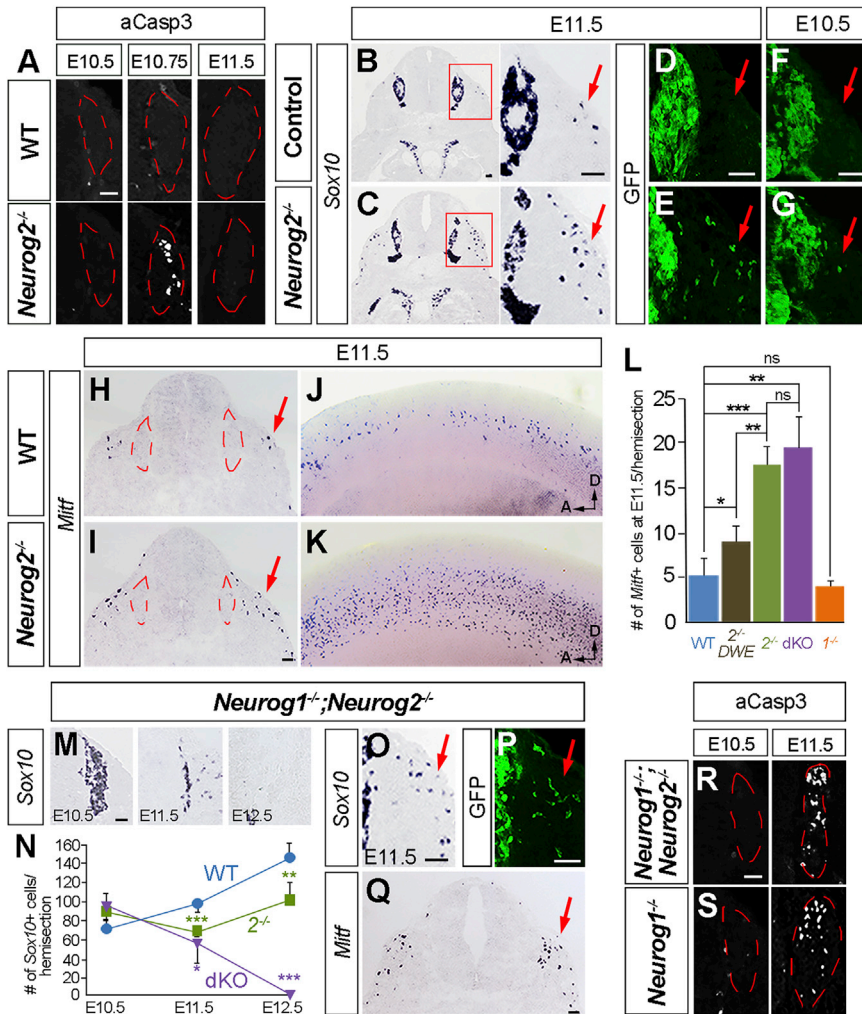


Figure 4. Cell Fate Switch toward the Melanocyte Lineage and/or Apoptosis Underlie the Depletion of Somatosensory Progenitor Pools in *Neurog1/2* Mutants

(A) Immunofluorescence staining for activated-Caspase3 (aCasp3) on thoracic DRG transverse sections from WT and *Neurog2*^{-/-} embryos at E10.5, E10.75, and E11.5.

(B and C) Representative images of *in situ* hybridizations for *Sox10* on thoracic DRG transverse sections from WT (B) and *Neurog2*^{-/-} (C) embryos at E11.5. Red frames indicate positions of the close-ups shown on the right.

(D–G) Immunofluorescence staining for GFP on thoracic DRG transverse sections from *Neurog2*^{+/+} (D and F) and *Neurog2*^{-/-} (E and G) embryos at E11.5 (D and E) and E10.5 (F and G). (H–K) Representative views of *in situ* hybridizations for *Mitf* on WT (H and J) and *Neurog2*^{-/-} (I and K) embryos on thoracic DRG transverse sections (H and I) or on whole-mount preparations (J and K) at E11.5.

(L) Quantification of *Mitf*⁺ melanoblasts in WT (blue column; n = 10), *2*^{-/-}-DWE (brown column; n = 5), *Neurog2*^{-/-} (*2*^{-/-}, green column; n = 10), *Neurog1*^{-/-};*Neurog2*^{-/-} (dKO, purple column; n = 5), or *Neurog1*^{-/-} (*1*^{-/-}, orange column; n = 4) embryos at E11.5. Data are represented as means ± SEM. n.s., not significant; **p < 0.01; ***p < 0.001.

(M) *In situ* hybridization for *Sox10* on thoracic DRG transverse sections from *Neurog1*^{-/-};*Neurog2*^{-/-} at E10.5, E11.5, and E12.5. (N) Quantitative time-course analyses of *Sox10*⁺ progenitors in the DRG of WT (blue curve), *Neurog2*^{-/-} (green curve), and *Neurog1*^{-/-};*Neurog2*^{-/-} (dKO, purple curve) between E10.5 and E12.5. Data are represented as means ± SEM. **p < 0.01; ***p < 0.001. (O–Q) *In situ* hybridizations for *Sox10* (O) or *Mitf* (Q) and immunofluorescence staining for GFP (P) on thoracic DRG transverse sections of *Neurog1*^{-/-};*Neurog2*^{-/-} embryos at E11.5.

(R and S) Immunofluorescence staining for activated-Caspase3 (aCasp3) on thoracic DRG transverse sections from *Neurog1*^{-/-};*Neurog2*^{-/-} (R) and *Neurog1*^{-/-} (S) embryos at E10.5 and E11.5. Red arrows in (B)–(I) and (O)–(Q) point to the dorsolateral migratory path. Red dotted lines in (A), (H), (I), (R) and (S) delimit the DRG. Scale bars, 50 μm.

See also Figures S3 and S4.

confirming and extending previous studies using Cre inducible lines (Zirlinger et al., 2002; Bartesaghi et al., 2019; Soldatov et al., 2019). Although this might appear paradoxical considering that *Neurog2* is expressed up to E11 (Sommer et al., 1996; Figure S2E), whereas second-wave progenitors differentiate until E13.5 (Lawson and Bischoff, 1979), this is consistent with the fact that all NCCs dedicated to the DRG have left the neural tube prior to E10.5 (Serbedzija et al., 1990) when *Neurog2*⁺ migrating cells are still detected (Figure S2E; Sommer et al., 1996). This, thus, supports a cell-autonomous role for *Neurog2* also in second-wave progenitors. However, in the light of the *Neurog1*^{-/-} and *Neurog1*^{-/-};*Neurog2*^{-/-} mutant phenotypes, *Neurog2* appears able to trigger neuronal differentiation in first-wave progenitors by itself, whereas in second-wave progenitors it is required to ensure integrity and on-time induction of *Neurog1* that, in turn, has the proneural role (Ma et al., 1999; Figure S4A).

Cell Fate Switch toward the Melanocyte Lineage and/or Apoptosis Underlie the Depletion of Somatosensory Progenitor Pools in *Neurog1/2* Mutants

We next aimed at determining the causes of the progenitor depletion observed in *Neurog2*^{-/-} mutants. Prompted by previous observations made at lumbar levels at E11.5 (Ma et al., 1999), we assessed cell death. At thoracic levels, although we could not detect any dying cells in mutant embryos at E10.5 and E11.5, we did so at an intermediate stage referred to as E10.75, indicating that apoptosis indeed contributes to this defect (Figure 4A). In parallel, we also noticed that the spatial distribution of the mutant *Sox10*⁺ NCCs in the region of the coalescing DRG was atypical. Indeed, in E11.5 *Neurog2*^{-/-} embryos, we systematically detected supernumerary *Sox10*⁺ cells at positions reminiscent of the “dorsolateral pathway” normally invaded by melanoblasts (Figures 4B and 4C; Hari et al., 2002,

2012; Mort et al., 2015). At this stage, many ectopic GFP+ cells were also observed in this region, occasionally already at E10.5 (Figures 4D–4G), prompting us to assess the melanocyte determinant *Mitf* (Opdecamp et al., 1997). At E11.5, although only few *Mitf*+ melanoblasts were detected in the trunk region of WT embryos, either on sections (Figure 4H) or on whole-mount preparations (Figure 4J), their numbers were massively expanded in *Neurog2*^{-/-} mutants (Figures 4I, 4K, and 4L). These data, thus, show that in the absence of *Neurog2*, a population of NCCs normally dedicated to the DRG adopts a melanocyte fate. Moreover, analyses on E11.5 *2*^{-/-}DWE animals revealed only a minor increase of the *Mitf*+ population (Figure 4L; Figures S3A and S3B), supporting that this cell fate conversion mainly concerned second-wave progenitors. It is of note that we did not observe any obvious ectopic GFP+ or supernumerary *Sox10*+ cells in other regions of *Neurog2*^{-/-} embryos, including in the sympathetic ganglia (Figures S3D and S3E; data not shown). Taken together, these data establish that the somatosensory progenitor depletion observed in the trunk of *Neurog2*^{-/-} embryos involves at least two processes, namely, apoptosis and cell fate conversion toward the melanocyte lineage (Figures S4A and S4B), both occurring during the narrow time window when *Neurog1* is undetectable and neurogenesis is blocked. It is of note that during the same period at cervical levels, *Neurog1* expression and neurogenesis have already started in the mutants (Ma et al., 1999). Therefore, temporal divergences in the “*Neurog2*-independent” upregulation of *Neurog1* expression may explain why no neuronal loss has been observed at this axial level. Nevertheless, because DRG development normally follows a temporal antero/posterior (A/P) gradient, this may rather reflect the existence of distinct spatial patterning modalities along this axis. Interestingly, such phenotypic divergences along the A/P axis have been also reported in the sympathetic chain of mutants for the proneural gene *Ascl1/Mash1* (Guillemot et al., 1993; Patryn et al., 2006).

The cell fate conversion undergone by a population of *Neurog2*-deficient NCCs echoes previous findings suggesting a role for *Neurog2* in specifying the somatosensory lineage. Indeed, *Neurog2* is the first *Neurog* gene induced in subsets of migrating NCCs (Sommer et al., 1996) that are biased toward the somatosensory lineage (Ziringer et al., 2002). Moreover, in gain-of-function experiments, *Neurog1/2* appear sufficient to trigger the production of sensory-like neurons at ectopic positions *in vivo* (Perez et al., 1999). We show here that the loss of *Neurog2* function has the opposite effect and redirects groups of somatosensory progenitors toward the melanocyte lineage, consistent with recent observations by Soldatov et al. (2019). This “inter-lineage” fate switch illustrates that pools of NCCs remain developmentally plastic *in vivo* and retain the competence to adopt alternative fates under certain circumstances (Vincentz et al., 2013; Nitzan et al., 2013; Soldatov et al., 2019), in line with the fact that many migrating NCCs appear multipotent (Baggiolini et al., 2015). Interestingly, the somatosensory and melanocyte lineages are developmentally linked, as notably illustrated by the reiterative role of the Wnt/beta-catenin pathway, which successively specifies first sensory progenitors then melanoblasts, likely through time-dependent regulation of *Neurog2* and *Mitf*, respectively (Hari et al., 2002, 2012; Lee et al., 2004;

Pavan and Raible, 2012). The fact that in *Neurog2*^{-/-} mutants some NCCs adopt a “later identity” suggests that, in this context, *Neurog2* acts as a “temporal fate transcription factor” (Kohwi and Doe, 2013).

Nevertheless, the somatosensory-to-melanocyte fate conversion did not concern all *Neurog*-deficient progenitors. Indeed, although some degenerate, others eventually induce *Neurog1* and differentiate, prompting us to assess their destiny in *Neurog1*^{-/-};*Neurog2*^{-/-} dKOs. Time-course analysis of numbers of *Sox10*+ NCCs in the DRG primordia of dKO expectedly revealed a slight increase at E10.5 but a significant decrease at E11.5 compared to WT, as in *Neurog2*^{-/-} embryos (Figures 4M and 4N). By E12.5, in contrast to *Neurog2*^{-/-} mutants, all *Sox10*+ NCCs were depleted in dKO (Figures 4M and 4N). As anticipated, this reflected a partial cell fate conversion toward the melanocytic lineage (Figures 4L and 4O–Q; see also Figure S3E). However, numbers of *Mitf*+ cells in dKOs were not statistically different from *Neurog2*^{-/-} mutants (Figure 4L). Instead, we found that cell death was greatly exacerbated in dKOs at E11.5 (Figure 4R). Consistent with this, in *Neurog1*^{-/-} single mutants we did not detect any supernumerary melanoblasts (Figure 4L; Figure S3C) but found that second-wave progenitors were progressively eliminated from E11.5 through apoptosis (Figure 4S; summarized in Figure S4C). Taken together, these data show that the additional loss of *Neurog1* function in a *Neurog2*^{-/-} mutant background triggers the rapid complete elimination of all NCC-derived somatosensory progenitors by an extended period of apoptosis, not an exacerbated fate switch phenotype (Figures S4D). This certainly illustrates heterogeneity among NCCs and suggests that some are early committed to the somatosensory lineage (Lo et al., 2005) and/or have lost the competence to interpret signals instructive for alternative fates and eventually die in case of abortive neurogenesis.

In conclusion, these findings illustrate heterogeneity among NCC-derived somatosensory progenitors and uncover a critical period of cell fate plasticity and vulnerability for this population. They also establish that the individual requirement of *Neurog2* in the forming DRG is more complex and broader than initially envisaged.

STAR★METHODS

Detailed methods are provided in the online version of this paper and include the following:

- KEY RESOURCES TABLE
- LEAD CONTACT AND MATERIALS AVAILABILITY
- EXPERIMENTAL MODEL AND SUBJECT DETAILS
- METHOD DETAILS
 - *In Situ* Hybridization (ISH)
 - Immunofluorescence Staining on Cryosections
- QUANTIFICATION AND STATISTICAL ANALYSIS
- DATA AND CODE AVAILABILITY

SUPPLEMENTAL INFORMATION

Supplemental Information can be found online at <https://doi.org/10.1016/j.celrep.2019.11.002>.

ACKNOWLEDGMENTS

We thank F. Guillemot, A. McMahon, and P. Topilko for *Neurog* mutants, *Wnt1Cre* transgenic animals, and *Egr2^{DT}* knockin mice, respectively; as well as J.F. Brunet, C. Goidis, L. Sommer, and M. Wegner for materials. This work was supported by Inserm, France; CNRS, France; Fondation pour la Recherche Médicale, France; Agence Nationale pour la Recherche, France; and University of Montpellier, France.

AUTHOR CONTRIBUTIONS

S.V., S.D., P.Cabochette., A.D., and A.P. performed the experiments. S.V., S.D., P.Cabochette., A.P., and P.Carroll. designed the experiments and interpreted the data. A.P. wrote the manuscript.

DECLARATION OF INTERESTS

The authors declare no competing interests.

Received: May 24, 2019

Revised: September 18, 2019

Accepted: October 30, 2019

Published: December 3, 2019

REFERENCES

- Andersson, E., Jensen, J.B., Parmar, M., Guillemot, F., and Björklund, A. (2006). Development of the mesencephalic dopaminergic neuron system is compromised in the absence of neurogenin 2. *Development* *133*, 507–516.
- Bachy, I., Franck, M.C., Li, L., Abdo, H., Pattyn, A., and Ernfors, P. (2011). The transcription factor *Cux2* marks development of an A-delta sublineage of TrkA sensory neurons. *Dev. Biol.* *360*, 77–86.
- Baggiolini, A., Varum, S., Mateos, J.M., Bettosini, D., John, N., Bonalli, M., Ziegler, U., Dimou, L., Clevers, H., Furrer, R., and Sommer, L. (2015). Premigratory and migratory neural crest cells are multipotent *in vivo*. *Cell Stem Cell* *16*, 314–322.
- Bartesaghi, L., Wang, Y., Fontanet, P., Wanderoy, S., Berger, F., Wu, H., Akkuratova, N., Bouçanova, F., Médard, J.J., Petitpré, C., et al. (2019). PRDM12 Is Required for Initiation of the Nociceptive Neuron Lineage during Neurogenesis. *Cell Rep.* *26*, 3484–3492.e4.
- Bhatt, S., Diaz, R., and Trainor, P.A. (2013). Signals and switches in Mammalian neural crest cell differentiation. *Cold Spring Harb. Perspect. Biol.* *5*, a008326.
- Chen, C.L., Broom, D.C., Liu, Y., de Nooij, J.C., Li, Z., Cen, C., Samad, O.A., Jessell, T.M., Woolf, C.J., and Ma, Q. (2006). *Runx1* determines nociceptive sensory neuron phenotype and is required for thermal and neuropathic pain. *Neuron* *49*, 365–377.
- Danielian, P.S., Muccino, D., Rowitch, D.H., Michael, S.K., and McMahon, A.P. (1998). Modification of gene activity in mouse embryos *in utero* by a tamoxifen-inducible form of Cre recombinase. *Curr. Biol.* *8*, 1323–1326.
- Desiderio, S., Vermeiren, S., Van Campenhout, C., Kricha, S., Malki, E., Richts, S., Fletcher, E.V., Vanwelden, T., Schmidt, B.Z., Henningfeld, K.A., et al. (2019). Prdm12 directs nociceptive sensory neuron development by regulating the expression of the NGF receptor TrkA. *Cell Rep.* *26*, 3522–3536.e5.
- Dupin, E., and Sommer, L. (2012). Neural crest progenitors and stem cells: from early development to adulthood. *Dev. Biol.* *366*, 83–95.
- Frank, E., and Sanes, J.R. (1991). Lineage of neurons and glia in chick dorsal root ganglia: analysis *in vivo* with a recombinant retrovirus. *Development* *111*, 895–908.
- George, L., Kasemeier-Kulesa, J., Nelson, B.R., Koyano-Nakagawa, N., and Lefcort, F. (2010). Patterned assembly and neurogenesis in the chick dorsal root ganglion. *J. Comp. Neurol.* *518*, 405–422.
- Guillemot, F., Lo, L.C., Johnson, J.E., Auerbach, A., Anderson, D.J., and Joyner, A.L. (1993). Mammalian achaete-scute homolog 1 is required for the early development of olfactory and autonomic neurons. *Cell* *75*, 463–476.
- Hadjab, S., Franck, M.C., Wang, Y., Sterzenbach, U., Sharma, A., Ernfors, P., and Lallemand, F. (2013). A local source of FGF initiates development of the unmyelinated lineage of sensory neurons. *J. Neurosci.* *33*, 17656–17666.
- Hari, L., Brault, V., Kléber, M., Lee, H.Y., Ille, F., Leimeroth, R., Paratore, C., Suter, U., Kemler, R., and Sommer, L. (2002). Lineage-specific requirements of beta-catenin in neural crest development. *J. Cell Biol.* *159*, 867–880.
- Hari, L., Miescher, I., Shakhova, O., Suter, U., Chin, L., Taketo, M., Richardson, W.D., Kessaris, N., and Sommer, L. (2012). Temporal control of neural crest lineage generation by Wnt/ β -catenin signaling. *Development* *139*, 2107–2117.
- Kohwi, M., and Doe, C.Q. (2013). Temporal fate specification and neural progenitor competence during development. *Nat. Rev. Neurosci.* *14*, 823–838.
- Lallemand, F., and Ernfors, P. (2012). Molecular interactions underlying the specification of sensory neurons. *Trends Neurosci.* *35*, 373–381.
- Lawson, S.N., and Biscoe, T.J. (1979). Development of mouse dorsal root ganglia: an autoradiographic and quantitative study. *J. Neurocytol.* *8*, 265–274.
- Lee, H.Y., Kléber, M., Hari, L., Brault, V., Suter, U., Taketo, M.M., Kemler, R., and Sommer, L. (2004). Instructive role of Wnt/ β -catenin in sensory fate specification in neural crest stem cells. *Science* *303*, 1020–1023.
- Liu, Y., and Ma, Q. (2011). Generation of somatic sensory neuron diversity and implications on sensory coding. *Curr. Opin. Neurobiol.* *21*, 52–60.
- Lo, L., Dormand, E.L., and Anderson, D.J. (2005). Late-emigrating neural crest cells in the roof plate are restricted to a sensory fate by GDF7. *Proc. Natl. Acad. Sci. USA* *102*, 7192–7197.
- Ma, Q., Fode, C., Guillemot, F., and Anderson, D.J. (1999). Neurogenin1 and neurogenin2 control two distinct waves of neurogenesis in developing dorsal root ganglia. *Genes Dev.* *13*, 1717–1728.
- Maro, G.S., Vermeren, M., Voiculescu, O., Melton, L., Cohen, J., Charnay, P., and Topilko, P. (2004). Neural crest boundary cap cells constitute a source of neuronal and glial cells of the PNS. *Nat. Neurosci.* *7*, 930–938.
- Moqrich, A., Earley, T.J., Watson, J., Andahazy, M., Backus, C., Martin-Zanca, D., Wright, D.E., Reichardt, L.F., and Patapoutian, A. (2004). Expressing TrkC from the TrkA locus causes a subset of dorsal root ganglia neurons to switch fate. *Nat. Neurosci.* *7*, 812–818.
- Mort, R.L., Jackson, I.J., and Patton, E.E. (2015). The melanocyte lineage in development and disease. *Development* *142*, 620–632.
- Nitzan, E., Pfaltzgraff, E.R., Labosky, P.A., and Kalcheim, C. (2013). Neural crest and Schwann cell progenitor-derived melanocytes are two spatially segregated populations similarly regulated by Foxd3. *Proc. Natl. Acad. Sci. USA* *110*, 12709–12714.
- Ohayon, D., Ventéo, S., Sonrier, C., Lafon, P.A., Garcès, A., Valmier, J., Rivat, C., Topilko, P., Carroll, P., and Pattyn, A. (2015). Zeb family members and boundary cap cells underlie developmental plasticity of sensory nociceptive neurons. *Dev. Cell* *33*, 343–350.
- Opdecamp, K., Nakayama, A., Nguyen, M.T., Hodgkinson, C.A., Pavan, W.J., and Arnheiter, H. (1997). Melanocyte development *in vivo* and in neural crest cell cultures: crucial dependence on the Mitf basic-helix-loop-helix-zipper transcription factor. *Development* *124*, 2377–2386.
- Pattyn, A., Guillemot, F., and Brunet, J.F. (2006). Delays in neuronal differentiation in Mash1/Ascl1 mutants. *Dev. Biol.* *295*, 67–75.
- Pavan, W.J., and Raible, D.W. (2012). Specification of neural crest into sensory neuron and melanocyte lineages. *Dev. Biol.* *366*, 55–63.
- Perez, S.E., Rebelo, S., and Anderson, D.J. (1999). Early specification of sensory neuron fate revealed by expression and function of neurogenins in the chick embryo. *Development* *126*, 1715–1728.
- Serbedzija, G.N., Fraser, S.E., and Bronner-Fraser, M. (1990). Pathways of trunk neural crest cell migration in the mouse embryo as revealed by vital dye labelling. *Development* *108*, 605–612.

Soldatov, R., Kaucka, M., Kastriti, M.E., Petersen, J., Chontorotzea, T., Eng-Imaier, L., Akkuratova, N., Yang, Y., Häring, M., Dyachuk, V., et al. (2019). Spatiotemporal structure of cell fate decisions in murine neural crest. *Science* 364, eaas9536.

Sommer, L., Ma, Q., and Anderson, D.J. (1996). Neurogenins, a novel family of atonal-related bHLH transcription factors, are putative mammalian neuronal determination genes that reveal progenitor cell heterogeneity in the developing CNS and PNS. *Mol. Cell. Neurosci.* 8, 221–241.

Vincentz, J.W., Firulli, B.A., Lin, A., Spicer, D.B., Howard, M.J., and Firulli, A.B. (2013). Twist1 controls a cell-specification switch governing cell fate decisions within the cardiac neural crest. *PLoS Genet.* 9, e1003405.

Zirlinger, M., Lo, L., McMahon, J., McMahon, A.P., and Anderson, D.J. (2002). Transient expression of the bHLH factor neurogenin-2 marks a subpopulation of neural crest cells biased for a sensory but not a neuronal fate. *Proc. Natl. Acad. Sci. USA* 99, 8084–8089.

STAR★METHODS

KEY RESOURCES TABLE

REAGENT or RESOURCE	SOURCE	IDENTIFIER
Antibodies		
Rabbit anti-TrkA	Millipore	Cat# 06-574; RRID: AB_310180
Goat anti-TrkB	R and D Systems	Cat# AF1494; RRID: AB_2155264
Goat anti TrkC	R and D Systems	Cat# AF1404; RRID: AB_2155412
Rabbit anti-CGRP	Sigma-Aldrich	Cat# C8198; RRID: AB_259091
Goat anti-c Ret	R and D Systems	Cat# AF482; RRID: AB_2301030
Chicken anti-GFP	Abcam	Cat# ab13970; RRID:AB_300798
Sheep anti-TH	Thermo Scientific	Cat# PA1-4679, RRID: AB_561880
Rabbit anti-Cleaved Caspase-3	Cell Signaling Technology	Cat# 9661; RRID: AB_2341188
Donkey anti-rabbit IgG, Alexa Fluor 594 conjugated	Molecular Probes	Cat# A-21207; RRID: AB_141637
Donkey anti-goat IgG, Alexa Fluor 488 conjugated	Molecular Probes	Cat# A-11055; RRID: AB_2534102
Donkey anti-sheep IgG, Alexa Fluor 568 conjugated	Molecular Probes	Cat# A-21099; RRID: AB_141474
Goat anti-chicken IgG, Alexa Fluor 488 conjugated	Molecular Probes	Cat# A-11039; RRID: AB_142924
Experimental Models: Organisms/Strains		
Mouse/ <i>DBZEB</i>	Ohayon et al., 2015	N/A
Mouse/ <i>Egr2^{gfp-DT/+}</i>	Maro et al., 2004	N/A
Mouse/ <i>Neurog1^{GFP/+}</i>	Ma et al., 1999	N/A
Mouse/ <i>Neurog2^{GFP/+}</i>	Andersson et al., 2006	N/A
Mouse/ <i>Wnt1-Cre</i>	Danielian et al., 1998	N/A
Software and Algorithms		
ImageJ	https://imagej.net/Welcome	RRID:SCR_003070
Microsoft Excel	https://www.microsoft.com/en-gb/	RRID:SCR_016137

LEAD CONTACT AND MATERIALS AVAILABILITY

Further information and request should be directed to and will be fulfilled by the Lead Contact, Alexandre Pattyn (alexandre.pattyn@inserm.fr). This study did not generate new unique materials or reagents.

EXPERIMENTAL MODEL AND SUBJECT DETAILS

Experiments described in this study were performed on mouse embryos from embryonic day (E) 9.5 to 18.5. Embryos were allocated to each experiment depending on their genotype which resulted in the comparison of genetically modified models with control littermates. 2-8 months old females and males of the *DBZEB* ([Ohayon et al., 2015](#)), *Egr2^{gfp-DT}* ([Maro et al., 2004](#)), *Neurog1^{-/-}* ([Ma et al., 1999](#)), *Neurog2^{-/-}* ([Andersson et al., 2006](#)), and *Wnt1Cre* ([Danielian et al., 1998](#)) strains were used for the breeding and were maintained and genotyped as previously described. They were provided *ad libitum* with standard mouse pellet food and water and housed at room temperature with a 12h light/dark cycle. All procedures were conducted according to the French Ministry of Agriculture and the European Community Council Directive no. 86/609/EEC, OJL 358. Protocols were validated by the Direction Départementale des Services Vétérinaires de l'Hérault (Certificate of Animal Experimentation no. 34-376).

METHOD DETAILS

In Situ Hybridization (ISH)

Antisense RNA probes for *DBH*, *gfp*, *Mitf*, *MrgprD*, *NeuroD*, *Neurog1*, *Neurog2*, *Runx1*, *SCG10*, *Sox10* and *TrpM8* were labeled using the Dig RNA labeling kit (Roche) and purified on G50 columns (GE Healthcare). For staining on cryosections, staged embryos were dissected out in cold Phosphate Buffer Saline (PBS), fixed for 2 hours at 4°C in 4% Paraformaldehyde(PFA)-PBS, cryoprotected in 20% Sucrose-PBS overnight (o.n.) at 4°C, embedded in OCT-compound (Tissue-Tek) and stored at -80°C until use. 12-14µm

transverse sections were done using a cryostat (Microm), placed on glass slides and stored at -20°C until use. For the staining procedure, slides were dried at room temperature (RT) for 20 minutes (min) and incubated o.n. at 70°C with the appropriate probes diluted 1/100-1/200 in the hybridization buffer (50% Formamide-10% Dextran Sulfate-1X Salt Solution-1mg/ml yeast tRNA-1X Denhardt's). They were washed twice 1 h at 70°C in 50% Formamide-1X Sodium/Sodium Citrate buffer-0.1% Tween 20. They were then washed 3 times 10 min at RT in MABT (1X Maleic acid buffer-0.1% Tween20), blocked in 20% Sheep Serum-2% Blocking Reagent (Roche)-MABT and incubated o.n. at 4°C with the anti-DIG antibody (Roche) diluted 1/2000 in the same buffer. Slides were washed 3 times for 10 min at RT in MABT, incubated twice for 15 min in buffer B3 (100mM Tris pH 9.5, 100mM NaCl, 50mM MgCl_2 , 0.1% Tween 20) and incubated with the NBT and BCIP substrates (Roche) diluted in B3. Slides were washed several times in water for 2 hours, dried at RT and mounted in Mowiol under coverslips.

For whole-mount *in situ* hybridization, staged embryos were dissected out in PBS, fixed o.n. at 4°C in 4% PFA-PBS, washed in PBS several times, progressively dehydrated in 100% EtOH and stored at -20°C until use. Embryos were progressively rehydrated in PBS-0.1% Tween20 (PBT), bleached in 2% H_2O_2 -PBT for 1 h, washed 3 times in PBT, treated with 10 $\mu\text{g/ml}$ Proteinase K-PBT for 10 min, rinsed in PBT and post-fixed in 4% PFA-0.2% Glutaraldehyde-PBT for 20 min at 4°C . They were then washed in PBT, pre-hybridized in the hybridization buffer (50% Formamide-1.3xSSC-5mM EDTA-50 $\mu\text{g/ml}$ yeast tRNA-0.5% CHAPS-2% Tween 20) for 1 h at 70°C , and hybridized o.n. at 70°C with the Dig-labeled *Mitf* antisense-RNA probe diluted 1/100 in the hybridization buffer. Embryos were then washed 2 times 30 min in hybridization buffer, rinsed in TST (10mM Tris pH 7.5, 0.5M NaCl, 0.1% Tween 20) and incubated twice 30 min at 37°C with 10 $\mu\text{g/ml}$ RNase A-TST. They were then washed in TST at RT and then twice in hybridization buffer for 30 min at 65°C . Embryos were then washed twice 10 min and the 1 h in MABT at RT, incubated in 20% Serum-MABT at RT for 1 h and incubated o.n. at 4°C with the anti-DIG antibody (Roche) diluted 1/2000 in 2% Serum-MABT. They were then washed in MABT for 3 days. They were rinsed several times in B3 and stained with the NBT/BCIP-B3 substrate solution (Roche). The staining was stopped by washing several times in PBT. Embryos were post-fixed in 4% PFA-PBT, washed in PBT, progressively transferred in 80% Glycerol-PBT and stored in the dark at 4% C.

Immunofluorescence Staining on Cryosections

Primary antibodies used in this study were as follows: Chicken anti-GFP (1/2000; Abcam); Goat anti-Ret (1/100; R and D Systems), TrkB (1/2000; R and D Systems) and TrkC (1/1000; R and D Systems); Rabbit anti-activated Caspase3 (1/2000; Cell Signaling), CGRP (1/500; Sigma-Aldrich) and TrkA (1/500; Millipore); Sheep anti-TH (1/1000; Thermo Scientific). Secondary antibodies (Molecular Probes) used were as follows; Donkey anti-rabbit IgG Alexa Fluor 594-conjugated (1/2000); Donkey anti-goat IgG Alexa Fluor 488-conjugated (1/1000); Donkey anti-sheep IgG Alexa Fluor 568-conjugated (1/2000) and Goat anti-chicken IgG Alexa Fluor 488-conjugated (1/1000).

For the staining procedure, slides were dried 20 min at RT, rinsed with PBS, blocked for 30 min at RT in 4% Serum-PBS-0.1% Triton X-100 and incubated o.n. at 4°C with the appropriate primary antibody(ies) diluted in the same buffer. Slides were then washed 3 times 10 min in PBS-0.1% Triton X-100 and incubated 1 h at RT with secondary antibody(ies) diluted in the same buffer. They were then washed 3 times 10 min at RT, mounted under coverslips in Mowiol and rapidly imaged. For Ret immunofluorescence staining, an antigen retrieval step was added at the beginning of the protocol. Slides were incubated 15 min at 68°C in 10mM Sodium Citrate Buffer-0.5% Tween-20 pH6 and were then cooled down at RT for 15 min. They were washed 3 times in PBS-0.1% Triton X-100 for 5 min and incubated in the blocking buffer.

Note that pictures showing ISH or immunofluorescence staining are representative of at least three independent animals.

QUANTIFICATION AND STATISTICAL ANALYSIS

Quantitative analyses were carried out on at least 3 independent animals of each genotype, except at E14.5 for which each side of 2 distinct embryos were counted. Thoracic DRG sections were processed either for ISH or immunofluorescence and imaged using a Zeiss microscope. Cell counts were performed on 6-8 sections for each animals depending on the stage using the ImageJ software. Only cells with a clearly identifiable nucleus were counted. Statistical analyses were performed using the Microsoft Excel software and expressed as mean \pm standard error to the mean (s.e.m). They were analyzed by two-sided Student t tests: $p < 0.05$ (*), $p < 0.01$ (**) and $p < 0.001$ (***) were considered as statistically significant. Note that no statistical methods were used to predetermine sample sizes, but numbers of animals and sections analyzed for each genotype and for each stage are consistent with those typically used in the field.

In Figures 3F, 3G, 3H, and 3J are presented extrapolated numbers of *NeuroD*⁺, *SCG10*⁺, *Neurog1*⁺ and *Sox10*⁺ cells from the first or the second neurogenic waves in WT or *Neurog2*^{-/-} mutants. "First-wave numbers" were respectively determined by analyzing and quantifying *DWE* and *2*^{-/-}*DWE* animals, in which only first wave progenitors are present (see also Figure 1) (Ohayon et al., 2015). "Second-wave numbers" were respectively deduced by subtracting the average numbers of cells counted in WT versus *DWE* animals on one hand, and in *Neurog2*^{-/-} versus *2*^{-/-}*DWE* embryos on the other hand.

DATA AND CODE AVAILABILITY

This study did not generate any dataset or code.